

One Map Does Not Fit All: Evaluating Saliency Map Explanation on Multi-Modal Medical Images

Weina Jin¹ Xiaoxiao Li² Ghassan Hamarneh¹

Abstract

Being able to explain the prediction to clinical end-users is a necessity to leverage the power of AI models for clinical decision support. For medical images, saliency maps are the most common form of explanation. The maps highlight important features for AI model's prediction. Although many saliency map methods have been proposed, it is unknown how well they perform on explaining decisions on multi-modal medical images, where each modality/channel carries distinct clinical meanings of the same underlying biomedical phenomenon. Understanding such *modality-dependent features* is essential for clinical users' interpretation of AI decisions. To tackle this clinically important but technically ignored problem, we propose the MSFI (Modality-Specific Feature Importance) metric to examine whether saliency maps can highlight modality-specific important features. MSFI encodes the clinical requirements on modality prioritization and modality-specific feature localization. Our evaluations on 16 commonly used saliency map methods, including a clinician user study, show that although most saliency map methods captured modality importance information in general, most of them failed to highlight modality-specific important features consistently and precisely. The evaluation results guide the choices of saliency map methods and provide insights to propose new ones targeting clinical applications.

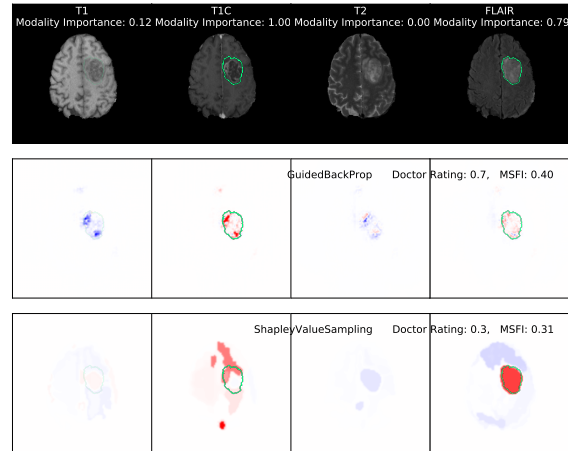


Figure 1. Multi-modality MRI and its saliency maps. The MRI shows a high-grade glioma. Although the brain tumor is visible on all modalities/pulse sequences of T1, T1C, T2 and FLAIR, multiple modalities present different signals which portray various compositions in the tissue. The radiographic features of contrast enhancement is most visible on T1C modality as hyperintense signal, and vasogenic edema appears as hyperintense signal abnormality on T2/FLAIR (UpToDate). Green contour is the ground truth tumor segmentation mask, with its intensity indicating the degree of importance a modality (Modality Importance) to model's prediction. We show saliency maps of a gradient-based method (GuidedBackProp) and a perturbation-based method (ShapleyValueSampling), with red color indicating the most important features, and blue the least important. We also present our proposed saliency map evaluation score — MSFI score and clinician rating from our user study, both rated on 3D images with [0, 1] range.

1. Introduction

Being able to explain decisions to users is a sought-after quality of deep learning-based models, particularly when considering their application in clinical decision support systems (Jin et al., 2020; He et al., 2019; Kelly et al., 2019). Explanations can help users verify the artificial intelligence (AI) model's decision (Ribeiro et al., 2016), calibrate their trust in AI assistance (Zhang et al., 2020; Bussone et al., 2015), identify potential biases (Caruana et al., 2015), make biomedical discoveries (Woo et al., 2017), meet ethical and legal requirements (Amann et al., 2020; gdp), and ultimately

¹School of Computing Science, Simon Fraser University, Burnaby, Canada ²Department of Electrical and Computer Engineering, The University of British Columbia, Vancouver, Canada. Correspondence to: Weina Jin <weinaj@sfu.ca>.

Evaluating Saliency Map Explanation on Multi-Modal Medical Images

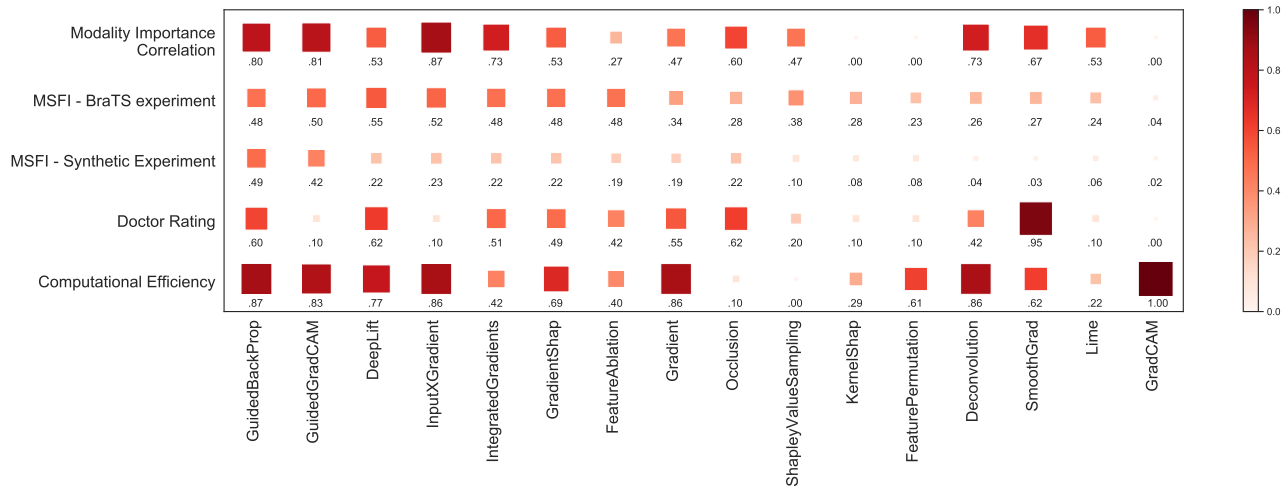


Figure 2. Comparison matrix of the evaluated 16 saliency map methods. The rows are evaluation metrics, and the columns are saliency map methods. All metrics are normalized to $[0, 1]$, and is indicated by the size of the square or the color. The darker or bigger a square is, the better a method is in that metric. We sort the methods in descending order according to their two summed MSFI scores (Row 2 + 3).

facilitate doctor-AI communication and collaboration to leverage the strengths of both (Wang et al., 2021; Topol, 2019; Carter & Nielsen, 2017). Prior user studies with physicians show that doctors tend to check the explanation to understand AI’s results when results are relevant to their own hypothesis or differential diagnosis (Xie et al., 2020), or to resolve conflicts when they disagree with AI (Cai et al., 2019).

Regarding medical imaging-related tasks, the most common and clinical end-user-friendly explanation is a saliency map (Jin et al., 2021; Reyes et al., 2020; Singh et al., 2020). It is also referred to, in the literature, as *sensitivity map*, *heatmap*, *feature attribution map*, or *feature importance map*. Saliency map methods are a group of feature attribution-based methods. They highlight image regions that are important for the model’s prediction, and encode the important scores for each image pixel by a color map overlaid on the input image (Fig. 1). A recent user study involving clinicians showed that knowing the important features that drive AI’s prediction is crucial, especially when clinicians need to compare AI’s decision to their own clinical judgment in cases of decision discrepancy (Tonekaboni et al., 2019). Many methods have been proposed to generate saliency maps in the explainable AI (XAI) and computer vision communities. These methods were mainly designed for and evaluated on natural images. Given the discrepancies between natural and medical images, the question of how well the saliency map methods explain decisions made on medical images, remains understudied.

One major discrepancy between natural and medical images is that a medical imaging study could include multiple im-

age modalities or channels (Martí-Bonmatí et al., 2010) and such modality-specific information is clinically meaningful. For example, different pulse sequences of magnetic resonance imaging (MRI) technique T1 weighted, T2 weighted, or fluid-attenuated inversion recovery (FLAIR) modalities; dual-modality imaging of positron emission tomography-computed tomography (PET-CT) (Beyer et al., 2002); CT images viewed at different levels and windows to observe different structures such as bones, lungs, and other soft tissues (Harris et al., 1993); multi-modal endoscopy imaging (Ray, 2017); Photographic (also called clinical), dermoscopic, and hyper-spectral images of a skin lesion (Kawahara et al., 2019; Zherebtsov et al., 2019); multiple stained microscopic or histopathological images (Long et al., 2020; Song et al., 2013). The signals from multiple image modalities capture different aspects of the same underlying cells, tissues, lesions, or organs.

Doctors rely on cross-modality comparison and combination to reason about a diagnosis or differential diagnosis. For instance, in a radiology report on MRI, radiologists usually observe and describe *anatomical* structures in T1 modality, and *pathological* changes in T2 modality (Cochard & Netter, 2012; Bitar et al., 2006); doctors can infer the composition of a lesion (such as fat, hemorrhage, protein, fluid) by combining its signals from different MRI modalities (Patel et al., 2016). In addition, some imaging modalities are particularly crucial for the diagnosis and management of certain diseases, such as a contrast-enhanced modality of CT or MRI in a tumor case, and diffusion-weighted imaging (DWI) modality MRI to a stroke case (Lansberg et al., 2000).

Method	Require access to model parameters	Model dependency	Computational efficiency
Activation-based	Yes	Deep neural networks	Fast
Gradient-based	Yes	Differentiable models	Fast
Perturbation-based	No	Model-agnostic	Slow

Table 1. Comparison of three groups of post-hoc saliency map methods

The uniqueness of multi-modal medical images brings up new and clinically relevant requirements for saliency map methods: The explanation needs to support the clinical user’s reasoning process towards decisions made based on multi-modal medical images, as stated above, and (to a certain degree) align with expert prior knowledge on what constitutes an important feature for each modality. Given the scarcity of work on saliency map evaluation for medical images, it is unclear whether existing methods will fulfill such requirement, and what needs to be improved in current methods to ensure their suitability for multi-modal medical images. One of the most conspicuous and clinically important questions to ask is:

Can the existing saliency map methods capture modality-specific important features that are aligned with clinical prior knowledge?

In this work, we give an exploratory answer to this question by proposing evaluation methods and conducting extensive comparisons with 16 commonly used saliency map methods. Specifically, we propose two evaluation methods/metrics, Modality Importance (MI) and Modality-Specific Feature Importance (MSFI), that reflect clinical knowledge on interpreting multi-modal medical images. The first metric, MI, corresponds to clinicians’ prioritization of multiple modalities. It uses Shapley value (Shapley, 1951) to determine the ground-truth importance for each image modality, and compares modality-wise summations of saliency map values with such a ground-truth. The second metric, MSFI, measures fine-grained clinical requirement on localizing features that are specific to each modality. It combines MI with feature localization masks as the ground-truth, and calculates the ratio of saliency map regions inside the segmentation map, weighted by MI. With the two metrics and a clinician user study, we conducted extensive evaluations on 16 saliency map methods that cover the most common activation-, gradient-, and perturbation-based approaches. The findings show that most saliency map methods can reflect the importance of a modality as a whole, but only a few methods could capture the modality-specific fine-grained features that meet clinical needs (Fig. 2). Our contributions in this work are:

1. We propound the clinically important problem of modality-specific saliency map explanation to the tech-

nical community;

2. We propose an evaluation metric MSFI that specifies clinical requirements on saliency maps from our physician user study. It assesses a given saliency map method’s ability to capture modality-specific features deemed important for an AI model’s decision. MSFI can be applied to any model and dataset with ground-truth feature localization masks only on test data.
3. We conduct extensive evaluation, including a doctor user study, on 16 commonly used saliency map methods. The assessments provide insights for XAI method selection and for proposing new XAI methods targeting clinical decision support systems that rely on multi-modal medical images.

2. Background and Related Work

2.1. Multi-Modality Learning

Approaches for building convolutional neural network (CNN) models that fuse multi-modal medical images can be divided into three categories: methods that fuse multi-modal features at the *input*-, *feature*-, and/or *decision*-levels (Xu, 2019). We focus on the most common setting for multi-modal medical imaging learning tasks: *input*-level multi-model image fusion (Shen et al., 2017), in which the multi-modal images are stacked as image channels and fed as input to a deep convolutional neural network. The modality-specific information is fused by summing up the weighted modality value in the first convolutional layer.

2.2. Saliency Map Methods

We focus on saliency map methods that are *post-hoc*. This group of methods is a type of proxy models that probe the model parameters and/or input-output pairs of an already deployed or trained black-box model. In contrast, the *ante-hoc* saliency map methods – such as attention mechanism – are predictive models with explanations baked into the training process. We leave out the *ante-hoc* methods because such explanations are entangled in its specialized model architecture, which would introduce confounders in the evaluation.

We describe the three major approaches to generating post-hoc saliency maps and how they have been applied to med-

ical imaging tasks. We review individual methods in each category in the Appendix. The key comparisons are highlighted in Table 1.

Activation-based methods, such as CAM (Class Activation Mapping) (Zhou et al., 2016), were proposed particularly for deep learning-based models. They aggregate neuron activation signals in a deep neural network, and visualize the signals in input space. Activation-based methods have been widely applied in medical imaging classification tasks such as chest X-Rays (Wang et al., 2017; Rajpurkar et al., 2018; Zech et al., 2018) and knee MRIs (Bien et al., 2018) to reveal what the models had learned and potential biases.

Gradient-based methods calculate the partial derivative of a prediction with respect to an input feature. The application of this group of methods to medical imaging tasks is also quite popular, such as for physicians’ quality assurance in brain tumor grading task (Pereira et al., 2018), for image biomarker discovery in neurodevelopment (Kawahara et al., 2017), for feature visualization on echocardiograms view classification (Madani et al., 2018).

Perturbation-based methods calculate the marginal probability of a feature as its attribute score by sampling from perturbed inputs. Since this class of methods need only probe the input-output pairs to generate an explanation, they do not require access to model parameters and thus are applicable to any black-box models. But they are usually computationally intensive as they require multiple passes through the model to acquire the perturbed input-output samples. Existing works applied different perturbation sampling methods such as occlusion on optical coherence tomography (OCT) images (Kermany et al., 2018), and Shapley values for Autism Spectrum Disorders biomarker discovery on MRI (Li et al., 2019).

In prior works, the saliency maps were usually presented as the sanity check of a model’s performance. Also, most of the saliency maps were on single-modal medical imaging-related tasks. Research work is lacking when the goal is to study a saliency map’s ability to capture modality-specific features, or to perform empirical evaluation of saliency maps for medical images.

2.3. Saliency Maps Evaluation

Evaluating explanation methods is challenging, because the ground-truth explanation is human users’ judgment. Such ground truth explanations are subjective and expensive to acquire especially from domain experts. To balance this, Doshi-Velez and Kim proposed three levels of evaluation: from the least expensive computational evaluation on proxy tasks, to human evaluation involving lay persons on simple tasks, to the most expensive domain expert evaluation on real tasks (Doshi-Velez & Kim, 2017). Our evaluations

cover both computational and domain expert evaluation.

Prior work proposed several computational evaluation metrics: Adebayo et al. proposed a sanity check on gradient-based explanations to evaluate their sensitivity to the randomization of training labels or model parameters (Adebayo et al., 2018). Among the 7 methods they inspected, only *Gradient* and *SmoothGrad* pass the sanity check. Other evaluation metrics such as *infidelity* (Yeh et al., 2019) and *Remove And Retrain* (Hooker et al., 2019) measure the changes in the output when perturbing the input. Object segmentation masks or bounding boxes can be used as a substitute ground-truth to quantify the localization capability of the saliency maps. Metrics such as intersection over union (IoU) are used to compare such a ground truth with the calculated saliency map (Taghanaki et al., 2019; Bau et al., 2017). Kim et al. conducted a controlled experiment on synthesized images with different levels of agreement between the ground-truth label and spurious features (Kim et al., 2018); their work inspired our synthetic experiment (Section 3.2.2).

3. Methods to Evaluate Multi-Modal Saliency Map Explanations

The overarching goal of the evaluation is to examine whether a saliency map method can reliably reveal features on multi-modal medical images that are clinically meaningful, given a well-trained model. Based on our physician user study (Section 4), we abstract such goal as two specific clinical requirements: modality prioritization, and modality-specific feature localization, which correspond to our evaluations at two granularity levels: **1) Modality Importance**: it measures a model’s overall importance of each modality as a whole; and **2) Modality-Specific Feature Importance (MSFI)**: it measures how well the saliency map can localize the modality-specific important features on each modality. Fig. 3 outlines the evaluation methods.

All evaluations are conducted on a brain tumor classification task to classify patients with gliomas into low-grade (LGG) or high-grade gliomas (HGG). We use the publicly available BraTS brain MRI dataset (Menze et al., 2015) with an input image $X \in \mathbb{R}^{M \times H \times W \times D}$, and a synthesized brain tumor dataset (Kim et al., 2021) with an input image $X \in \mathbb{R}^{M \times H \times W}$, where M is the number of modalities and H, W, D are width, height, and depth for each single modality MR image. Both datasets include $M = 4$ MRI modalities (or pulse sequences) of T1, T1C (contrast enhancement), T2, and FLAIR.

3.1. Modality Importance (MI)

As stated in Section 1, each modality may carry different information for a model’s prediction. We use Modality Importance to abstract and simplify such notion. It uses im-

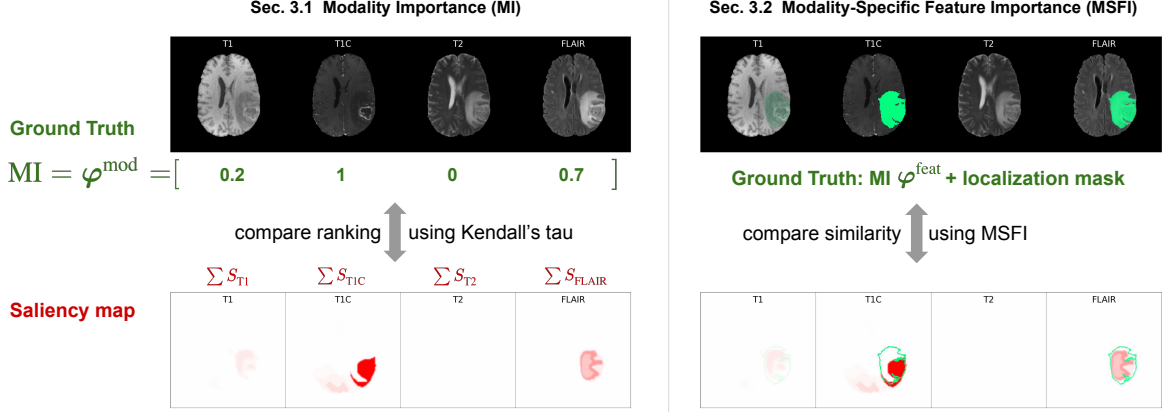


Figure 3. The computational evaluation methods.

importance scores to prioritize how critical a whole modality is to the overall prediction. To determine the ground-truth Modality Importance, we use Shapley value from cooperative game theory (Shapley, 1951), due to its desirable properties such as efficiency, symmetry, linearity, and marginalism. In a set of M modalities, Shapley value treats each modality m as a player in a cooperative game play. It is the unique solution to fairly distribute the total contributions (in our case, the model performance) across each individual modality m .

Shapley value-based ground-truth We define the modality Shapley value φ_m to be the ground truth Modality Importance score for a modality m . It is calculated as:

$$\varphi_m(v) = \sum_{c \subseteq \mathcal{M} \setminus \{m\}} \frac{|c|!(M - |c| - 1)!}{M!} (v(c \cup \{m\}) - v(c))$$

where v is the modality-specific performance metric, and $\mathcal{M} \setminus \{m\}$ denotes all modality subsets not including modality m . In our evaluation, v is calculated as the prediction model accuracy on the test set. To calculate the performance due to a subset of modalities, we set all values in a modality that is not included in the subset as 0. We denote such modality Shapley value as φ_m^{mod} . We also explored a variant setting where we replace the non-zero values of an ablated modality by sampling from the non-lesion regions. Since such resultant Shapley values had the same ranking and magnitude across modalities, we adopt the setting of zero replacement for simplicity.

Evaluation To compare the saliency maps' modality importance value with the aforementioned ground-truth, for each saliency map method, we generate and post-process (Section 5.2) the saliency maps, and calculate the *estimated modality importance* as the sum of all positive values of the saliency map for that modality. *MI Correlation* measures the MI ranking agreement between the ground-truth and the

estimated MI, calculated using Kendall's Tau-b correlation on the test set.

3.2. Modality-Specific Feature Importance (MSFI)

The above Modality Importance prioritizes the important modality, but it is a coarse measurement and does not examine the particular image features within each modality. To inspect the fine-grained features within each modality image, we further propose the MSFI (Modality-Specific Feature Importance) metric. It combines two types of ground-truth information: the modality prioritization information MI, and the feature localization masks/bounding boxes. MSFI is the portion of saliency map values inside the ground truth feature localization mask for each modality, weighted by the normalized MI value φ_m .

$$\hat{\text{MSFI}} = \sum_m \varphi_m \frac{\sum_i \mathbb{1}(L_m^i > 0) \odot S_m^i}{\sum_i S_m^i} \quad (1)$$

$$\text{MSFI} = \frac{\hat{\text{MSFI}}}{\sum_m \varphi_m} \quad (2)$$

where S_m is the saliency map for modality m , with i denoting the spatial location. L_m is the ground truth feature localization masks/bounding boxes for modality m , with $L_m^i > 0$ outlining the spatial location of the feature. $\mathbb{1}$ is the indicator function that selects the saliency map values within the feature mask. φ_m is the ground truth Modality Importance value for modality m that is normalized to range $[0, 1]$. $\hat{\text{MSFI}}$ is unnormalized, and MSFI is the normalized metric with the range of $[0, 1]$. In our evaluation, we use $S_m^i = \mathbb{1}(S_m^i > 0) \odot \hat{S}_m^i$, where \hat{S}_m^i is the saliency map that only includes positive values. A higher MSFI score (Fig. 1) indicates a saliency map that better captures the important modalities and their localized features. Unlike other common metrics such as IoU, MSFI is less dependent on either

saliency map signal intensity, or area of the ground truth localization mask, which makes it a robust metric. Next, we describe our evaluation experiments of applying MSFI on a real dataset (BraTS) and a synthetic dataset.

3.2.1. MSFI EVALUATION ON A MEDICAL IMAGE DATASET OF REAL PATIENTS

We use the same BraTS data and model as in Section 3.1. To make the ground truth represent the modality-specific feature localization information, we slightly change the way to compute the modality Shapley value φ_m . We define φ_m^{feat} to be the importance of the localized feature on each modality. Specifically, instead of ablating the modality as a whole to create a modality subset c , we zero-ablate only the localized feature region defined by the segmentation map. We calculate MSFI score with the new ground truth φ_m^{feat} .

3.2.2. MSFI EVALUATION ON A SYNTHESIZED DATASET WITH KNOWN GROUND TRUTH

To better control the Modality Importance ground truth, in this second evaluation experiment, we use a synthetic multi-modal medical image dataset on the same brain tumor HGG versus LGG classification task. We use the GAN-based (generative adversarial network) tumor synthesis model developed by Kim et al. (Kim et al., 2021) to control the shape and coarseness of the tumor textural patterns, and generate two types of tumors mimicking LGG and HGG (Appendix Fig.4) as well as their segmentation maps. The two controllable features are discriminative for tumor grading based on the literature (ho Cho et al., 2018).

To make the discriminative features modality specific, we select two modalities, and assign them different weights to control the degree at which the discriminative features align or agree with the ground-truth labels. The unselected modalities have 0 weights, i.e., they do not contain class discriminative features. For the selected two modalities, we set tumor features on TIC to have 100% alignment with the ground-truth label, and FLAIR to have a probability of 70% alignment, i.e., the tumor features on FLAIR corresponds to the correct label with 70% probability. In this way, the model can choose to pay attention to either the less noisy TIC modality, or to the more noisy FLAIR modality, or to both. To determine their relative importance as the ground truth Modality Importance, we test the well-trained model on two datasets:

TIC dataset: The dataset shows tumors only (without brain background) on all modalities. And the tumor visual features has **100%** alignment with ground-truth on **TIC** modality, and 0% alignment on **FLAIR**. Its test accuracy is denoted as Acc_{TIC} .

FLAIR dataset: The dataset shows tumors only on all

modalities. And the tumor visual features has **100%** alignment with ground-truth on **FLAIR** modality, and 0% alignment on **TIC**. Its test accuracy is denoted as $\text{Acc}_{\text{FLAIR}}$.

The performance A_{TIC} and A_{FLAIR} indicate the degree of model reliance on that modality to make prediction. We then use them as the ground truth Modality Importance.

4. Physician User Study

In addition to the above computational ground-truth, we conduct a user study with doctors to acquire the domain expert ground-truth. The recruited neurosurgeon was introduced to the AI assistant on classifying LGG versus HGG. The doctor was presented two MRI cases and their corresponding saliency maps from the 16 evaluated methods. The doctor was asked to estimate a percentage of match between highlighted saliency areas and his/her clinical judgment on the important features to classify LGG/HGG, and comment on each one. Currently we have recruited one neurosurgeon, and efforts to involve additional neurosurgeons/neuro-radiologists in the study are ongoing. The user study is approved by Research Ethics Board of the university (Study No.: H20-03588). The interview question list is in the Appendix.

5. Implementation Details

5.1. Data and Model

Our methods are validated on a real clinical dataset — BraTS 2020 dataset¹ and a synthetic dataset for sanity check (as described in Section 3.2.2). The multi-modal images in BraTS dataset are pre-registered and pre-processed. The BraTS dataset includes tumor grade labels of LGG or HGG (with the number of cases of LGG: HGG = 76 : 293), and tumor segmentation masks.

Since post-hoc saliency map methods need to explain an already trained model, we built a VGG-like 3D CNN that receives multi-modal 3D MR images $X \in \mathbb{R}^{4 \times 240 \times 240 \times 155}$. We used five-fold cross validation. We denote the model tested on fold i as Fold i model, for $i \in \{1, 2, \dots, 5\}$. From the remaining data in the other folds, we took around 20% for validation and the rest for training. We used weighted sampler to handle the imbalanced data, with a learning rate = 0.0005, batch size = 4, and training epoch of 32, 49, 55, 65, 30 for each fold selected by the validation data. The accuracies of the five folds are $87.81 \pm 3.40\%$ (mean \pm std) (Table 2).

For the synthetic brain tumor dataset, we first fitted a classification model the synthesized brain images by fine-tuning

¹Multimodal Brain Tumor Segmentation Challenge <http://www.med.upenn.edu/cbica/brats2020/data.html>

the pre-trained DenseNet121 that receives 2D multi-modal MRI input slices of $X \in \mathbb{R}^{4 \times 256 \times 256}$, with the number of cases of LGG : HGG = 1 : 1. We used the same training strategies as described above. The model achieves $95.70 \pm 0.06\%$ accuracy on the test set. The saliency maps were generated on a test set with the same ground-truth alignment probability as its training set.

We used PyTorch² and Monai API³ for model training, and Captum⁴ for generating post-hoc saliency maps. The computational efficiency/speed reported in Fig. 2 were the inverse normalized log mean computational time using a computer with 1 GTX Quadro 24GB GPU and 8 CPU cores.

5.2. Post-Processing Saliency Maps

Before evaluating and visualizing the saliency maps, we normalized them by first capping the top 1% outlying values (following (Smilkov et al., 2017)). We focused on the positive values of the saliency maps as they are interpreted as the evidence towards the model decision (a.k.a. importance scores), thus set the negative values (features against decision) to zeros. We normalized the values of the saliency maps to $[0, 1]$ for easier visualization and comparison.

6. Evaluation Result and Discussion

6.1. Modality Importance

The ground-truth modality Shapley value φ_m^{mod} of each modality is shown in Table 2. We notice Fold 3 model has a different modality importance ranking, and the importance magnitude is significantly smaller than the rest models. This may be due to the model is not well-trained (its performance is the worst). Fig. 4-top shows the ranking similarity between the ground truth and the saliency maps, and the summarized mean is visualized in Fig. 2. Except the saliency map methods (GradCAM, KernelSHAP, Feature Permutation) that can only generate one same map for all modalities, the majority saliency map methods could correctly reflect the important modality for the model’s decision in general, but with large variations on individual data points.

6.2. Modality-Specific Feature Importance

6.2.1. MSFI RESULTS ON BRATS DATASET

The Spearman correlation between doctor’s rating and MSFI score is 0.53 ($p=0.001$), indicating a moderate correlation between the computational metric and domain expert ground truth. Fig.1 gives some qualitative visualization of saliency

²<http://pytorch.org>

³<http://monai.io>

⁴<http://captum.ai>

	Fold 1	Fold 2	Fold 3	Fold 4	Fold 5
T1	0.03	-0.04	0.028	-0.07	-0.01
T1C	0.55	0.53	<i>0.012</i>	0.32	0.37
T2	-0.04	0.05	-0.007	0.14	0.13
FLAIR	<i>0.16</i>	<i>0.16</i>	-0.005	<i>0.24</i>	<i>0.21</i>
Acc	90.54%	90.54%	82.43%	85.14%	90.41%

Table 2. The Modality Importance ground truth φ_m^{mod} for each model on BraTS dataset. The first and second important modalities are bolded and italicized respectively. We also list the individual model performance on test set accuracy.

Modality	Fold 1	Fold 2	Fold 3	Fold 4	Fold 5
T1	0.01	-0.01	-0.01	-0.02	-0.001
T1C	0.22	0.36	0.09	0.14	0.191
T2	-0.02	0.04	0.01	0.02	-0.003
FLAIR	<i>0.17</i>	<i>0.12</i>	<i>0.03</i>	<i>0.10</i>	<i>0.060</i>

Table 3. The modality-specific feature importance ground truth φ_m^{feat} for each model on BraTS dataset.

maps with the two scores⁵. A full visualization of all saliency maps and their corresponding doctor ratings/MSFI scores are in the Appendix.

The ground-truth modality Shapley value φ_m^{feat} of each modality is shown in Table 3. It has the same trend as the φ_m^{mod} value. And the rankings of both φ_m align with doctor’s prior clinical knowledge, as quoted by the doctor in the user study:

“Many of us just look at FLAIR and TIC. 90% of my time is on the TIC, and then I will spend 2% on each of the other modalities.”

In addition, doctors use such modality prioritization information and modality-specific feature localization to judge the quality of saliency maps. These clinical requirements on saliency maps are incorporated into the MI and MSFI metrics.

“This one (Feature Ablation saliency map) is not bad on the FLAIR (modality), it (the tumor) is very well detected. I wouldn’t give it a perfect mark, because I would like it to prioritize the TIC (modality) instead. But I’ll give it (a score of) 75 (out of 100).”

The average MSFI score for each saliency map method is in the middle to the lower range, with a large variation among

⁵The 3D saliency maps used in the physician user study can be viewed at: <http://vimeo.com/channels/1705604>

Evaluating Saliency Map Explanation on Multi-Modal Medical Images

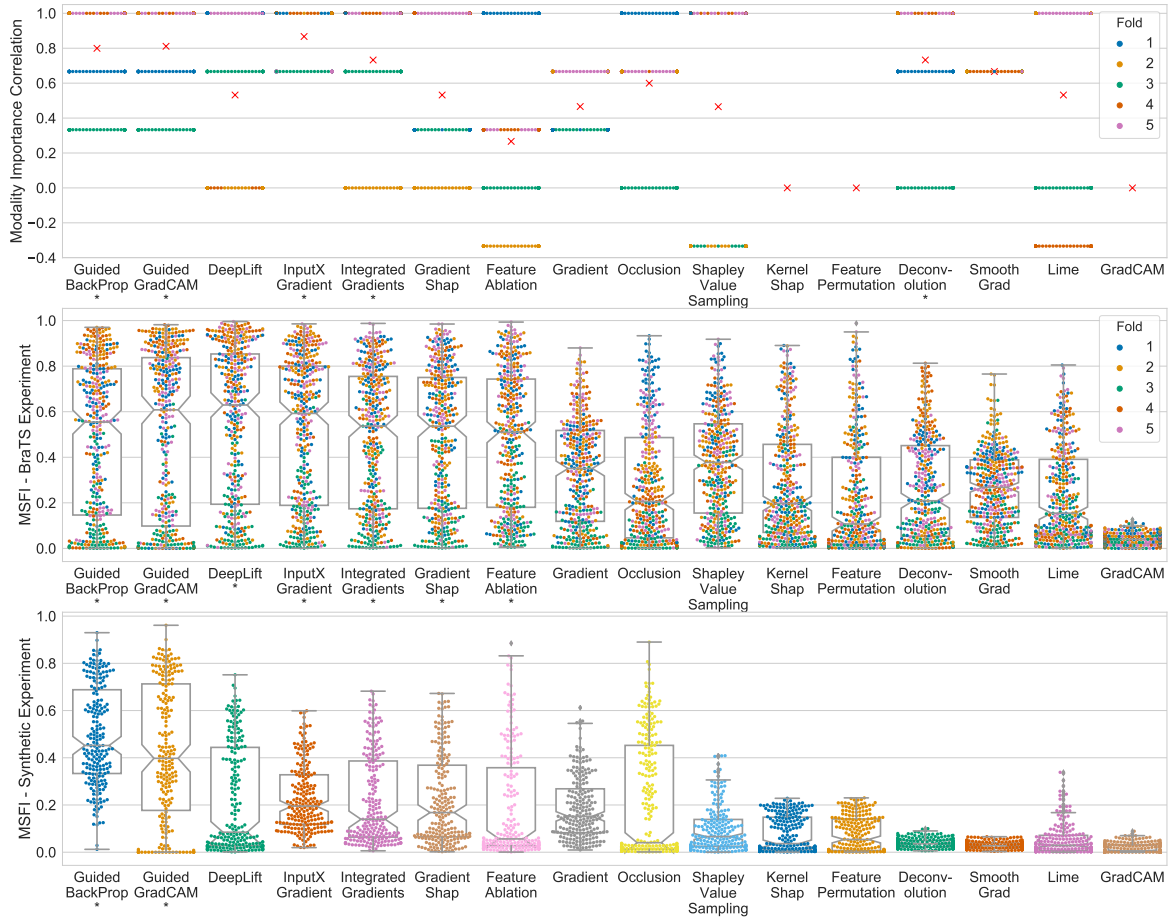


Figure 4. Modality Importance correlation and MSFI scores of the evaluated 16 saliency map methods. The three swarm plots show the evaluation score distribution for MI correlation (top), MSFI on BraTS dataset (middle), and MSFI on synthetic dataset (bottom). X-axis shows each saliency map method. Y-axis shows the evaluation metric, and a higher score means better alignment of a saliency map with the clinical requirements on modality prioritization (MI) and feature localization (MSFI). Each dot is a data sample in the test set, with means indicated by \times (top), or medians indicated by box plot (middle & bottom). There was a statistically significant difference among the 16 saliency map methods for each subplot as determined by Friedman test, and the top methods have their name marked with * (determined by not significantly different from the top two means using post-hoc Nemenyi test).

individual test data (Fig. 2, Fig. 4-middle). Both the computation evaluation and the doctor user study indicate the existing off-the-shelf saliency map methods may not fulfill the clinical requirements on modality-specific feature localization. Even for methods that have the best mean MSFI scores (around 0.5) such as DeepLift or GuideGradCAM, the MSFI score for individual data points vary across the full range from 0 to 1. Such performance fluctuation of saliency maps may be due to model training (most green dots have very low MSFI score, which is from the least performance model), prediction uncertainty, or weakness of the saliency map method. In our user study, the doctor relied on saliency maps to judge model’s prediction quality. Given the large variants, it is unknown whether saliency map can reliably support clinical users’ judgment on decision quality (Viviano et al., 2021), and further study needs to inspect the

cause of saliency map performance variation.

6.2.2. MSFI RESULTS ON SYNTHESIZED DATASET

Based on the synthetic dataset setting and the test result $\text{Acc}_{\text{T1C}} = 0.99$, $\text{Acc}_{\text{FLAIR}} = 0$, the ground truth Modality Importance is 1 for T1C, and 0 for the rest modalities. Using this and the segmentation maps, the calculated MSFI score distribution for the test set is shown in Fig. 4-bottom. Most of the saliency map methods can not correctly highlight the ground truth tumor regions on T1C modality, with *GuidedBackProp* and *GuidedGradCAM* outperform the rest.

7. Conclusion

Explainable AI is an indispensable component when implementing AI as clinical assistant on medical image-related tasks. In this work, we propose a clinically important but technically ignored problem: explaining model’s decisions on multi-modal medical images to clinical users. We propose two evaluation metrics MI (Modality Importance) and MSFI (Modality-Specific Feature Importance). The MI metric indicates the alignment of clinical evidence relying on a certain modality, and further enables the calculation for MSFI that measures saliency map quality with respect to clinical requirements on modality prioritization and feature localization. MSFI metric can be used to evaluate and select the most clinically relevant saliency map method for deployment. Our evaluation on BraTS and synthetic datasets reveals that existing saliency map methods may not be capable to reflect such modality-specific feature importance information. Future work may incorporate MSFI into the objective function, and propose new saliency map methods to precisely reflect the model’s learned representations and the clinical prior knowledge.

Acknowledgement

We thank Yiqi Yan for his earlier work on Brain Tumor Classification task. We thank Sunho Kim for his generous support to applying his work (Kim et al., 2021) on brain tumor MRI synthesis. We thank Shahab Aslani for the helpful discussions. This study is funded by BC Cancer Foundation-BrainCare BC Fund.

References

The impact of the General Data Protection Regulation (GDPR) on artificial intelligence. doi: 10.2861/293. URL <http://www.europarl.europa.eu/thinktank>.

Adebayo, J., Gilmer, J., Muelly, M., Goodfellow, I., Hardt, M., and Kim, B. Sanity checks for saliency maps. In Bengio, S., Wallach, H., Larochelle, H., Grauman, K., Cesa-Bianchi, N., and Garnett, R. (eds.), *Advances in Neural Information Processing Systems*, volume 31. Curran Associates, Inc., 2018. URL <https://proceedings.neurips.cc/paper/2018/file/294a8ed24b1ad22ec2e7efea049b8737-Paper.pdf>.

Amann, J., Blasimme, A., Vayena, E., Frey, D., and Madai, V. I. Explainability for artificial intelligence in healthcare: a multidisciplinary perspective. *BMC Medical Informatics and Decision Making*, 20(1):310, dec 2020. ISSN 14726947. doi: 10.1186/s12911-020-01332-6. URL <https://bmcmmedinformdecismak>.

biomedcentral.com/articles/10.1186/s12911-020-01332-6.

Bau, D., Zhou, B., Khosla, A., Oliva, A., and Torralba, A. Network dissection: Quantifying interpretability of deep visual representations. In *Computer Vision and Pattern Recognition*, 2017.

Beyer, T., Townsend, D. W., and Blodgett, T. M. Dual-modality PET/CT tomography for clinical oncology. *Q J Nucl Med*, 46(1):24–34, Mar 2002.

Bien, N., Rajpurkar, P., Ball, R. L., Irvin, J., Park, A., Jones, E., Bereket, M., Patel, B. N., Yeom, K. W., Shpanskaya, K., Halabi, S., Zucker, E., Fanton, G., Amanatullah, D. F., Beaulieu, C. F., Riley, G. M., Stewart, R. J., Blankenberg, F. G., Larson, D. B., Jones, R. H., Langlotz, C. P., Ng, A. Y., and Lungren, M. P. Deep-learning-assisted diagnosis for knee magnetic resonance imaging: Development and retrospective validation of MRNet. *PLOS Medicine*, 15(11):e1002699, nov 2018. ISSN 1549-1676. doi: 10.1371/journal.pmed.1002699. URL <http://dx.plos.org/10.1371/journal.pmed.1002699>.

Bitar, R., Leung, G., Perng, R., Tadros, S., Moody, A. R., Sarrazin, J., McGregor, C., Christakis, M., Symons, S., Nelson, A., and Roberts, T. P. MR pulse sequences: What every radiologist wants to know but is afraid to ask. *RadioGraphics*, 26(2):513–537, March 2006. doi: 10.1148/rg.262055063. URL <https://doi.org/10.1148/rg.262055063>.

Bussone, A., Stumpf, S., and O’Sullivan, D. The role of explanations on trust and reliance in clinical decision support systems. In *2015 International Conference on Healthcare Informatics*, pp. 160–169, 2015. doi: 10.1109/ICHI.2015.26.

Cai, C. J., Winter, S., Steiner, D., Wilcox, L., and Terry, M. "hello ai": Uncovering the onboarding needs of medical practitioners for human-ai collaborative decision-making. *Proc. ACM Hum.-Comput. Interact.*, 3(CSCW), November 2019. doi: 10.1145/3359206. URL <https://doi.org/10.1145/3359206>.

Carter, S. and Nielsen, M. Using artificial intelligence to augment human intelligence. *Distill*, 2(12), December 2017. doi: 10.23915/distill.00009. URL <https://doi.org/10.23915/distill.00009>.

Caruana, R., Lou, Y., Gehrke, J., Koch, P., Sturm, M., and Elhadad, N. Intelligible models for healthcare: Predicting pneumonia risk and hospital 30-day readmission. In *Proceedings of the ACM SIGKDD International Conference on Knowledge Discovery and Data Mining*, volume 2015-Augus, pp. 1721–1730, New York, New York,

- USA, aug 2015. Association for Computing Machinery. ISBN 9781450336642. doi: 10.1145/2783258.2788613. URL <http://dl.acm.org/citation.cfm?doid=2783258.2788613>.
- Cochard, L. R. and Netter, F. H. *Netters introduction to imaging*. Elsevier Saunders, 2012.
- Doshi-Velez, F. and Kim, B. Towards a rigorous science of interpretable machine learning, 2017.
- Harris, K., Adams, H., Lloyd, D., and Harvey, D. The effect on apparent size of simulated pulmonary nodules of using three standard ct window settings. *Clinical Radiology*, 47(4):241–244, 1993. ISSN 0009-9260. doi: [https://doi.org/10.1016/S0009-9260\(05\)81130-4](https://doi.org/10.1016/S0009-9260(05)81130-4). URL <https://www.sciencedirect.com/science/article/pii/S0009926005811304>.
- He, J., Baxter, S. L., Xu, J., Xu, J., Zhou, X., and Zhang, K. The practical implementation of artificial intelligence technologies in medicine. *Nature Medicine*, 25(1):30–36, January 2019. doi: 10.1038/s41591-018-0307-0. URL <https://doi.org/10.1038/s41591-018-0307-0>.
- ho Cho, H., hak Lee, S., Kim, J., and Park, H. Classification of the glioma grading using radiomics analysis. *PeerJ*, 6: e5982, November 2018. doi: 10.7717/peerj.5982. URL <https://doi.org/10.7717/peerj.5982>.
- Hooker, S., Erhan, D., Kindermans, P.-J., and Kim, B. A benchmark for interpretability methods in deep neural networks. In *NeurIPS*, pp. 9734–9745, 2019. URL <http://papers.nips.cc/paper/9167-a-benchmark-for-interpretability-methods-in-deep-neural-networks>.
- Jin, W., Fatehi, M., Abhishek, K., Mallya, M., Toyota, B., and Hamarneh, G. Artificial intelligence in glioma imaging: challenges and advances. *Journal of Neural Engineering*, 17(2):21002, apr 2020. doi: 10.1088/1741-2552/ab8131.
- Jin, W., Fan, J., Gromala, D., Pasquier, P., and Hamarneh, G. EUCA: A practical prototyping framework towards end-user-centered explainable artificial intelligence, 2021.
- Kawahara, J., Brown, C. J., Miller, S. P., Booth, B. G., Chau, V., Grunau, R. E., Zwicker, J. G., and Hamarneh, G. Brainnetcnn: Convolutional neural networks for brain networks; towards predicting neurodevelopment. *NeuroImage*, 146:1038–1049, 2017. ISSN 1053-8119. doi: <https://doi.org/10.1016/j.neuroimage.2016.09.046>. URL <https://www.sciencedirect.com/science/article/pii/S1053811916305237>.
- Kawahara, J., Daneshvar, S., Argenziano, G., and Hamarneh, G. Seven-point checklist and skin lesion classification using multitask multimodal neural nets. *IEEE Journal of Biomedical and Health Informatics*, 23(2):538–546, 2019. doi: 10.1109/JBHI.2018.2824327.
- Kelly, C. J., Karthikesalingam, A., Suleyman, M., Corrado, G., and King, D. Key challenges for delivering clinical impact with artificial intelligence. *BMC Medicine*, 17(1):195, 2019. ISSN 1741-7015. doi: 10.1186/s12916-019-1426-2. URL <https://doi.org/10.1186/s12916-019-1426-2>.
- Kermany, D. S., Goldbaum, M., Cai, W., Valentim, C. C., Liang, H., Baxter, S. L., McKeown, A., Yang, G., Wu, X., Yan, F., Dong, J. J., Prasadha, M. K., Pei, J., Ting, M. M. Y., Zhu, J., Li, C., Hewett, S., Dong, J. J., Ziyar, I., Shi, A., Zhang, R., Zheng, L., Hou, R., Shi, W., Fu, X., Duan, Y., Huu, V. A., Wen, C., Zhang, E. D., Zhang, C. L., Li, O., Wang, X., Singer, M. A., Sun, X., Xu, J., Tafreshi, A., Lewis, M. A., Xia, H., and Zhang, K. Identifying Medical Diagnoses and Treatable Diseases by Image-Based Deep Learning. *Cell*, 172(5):1122–1131.e9, feb 2018. ISSN 10974172. doi: 10.1016/j.cell.2018.02.010. URL <http://www.ncbi.nlm.nih.gov/pubmed/29474911https://linkinghub.elsevier.com/retrieve/pii/S0092867418301545https://doi.org/10.1016/j.cell.2018.02.010>.
- Kim, B., Wattenberg, M., Gilmer, J., Cai, C., Wexler, J., Viegas, F., and sayres, R. Interpretability beyond feature attribution: Quantitative testing with concept activation vectors (TCAV). In Dy, J. and Krause, A. (eds.), *Proceedings of the 35th International Conference on Machine Learning*, volume 80 of *Proceedings of Machine Learning Research*, pp. 2668–2677. PMLR, 10–15 Jul 2018. URL <http://proceedings.mlr.press/v80/kim18d.html>.
- Kim, S., Kim, B., and Park, H. Synthesis of brain tumor multicontrast MR images for improved data augmentation. *Medical Physics*, March 2021. doi: 10.1002/mp.14701. URL <https://doi.org/10.1002/mp.14701>.
- Lansberg, M. G., Albers, G. W., Beaulieu, C., and Marks, M. P. Comparison of diffusion-weighted MRI and CT in acute stroke. *Neurology*, 54(8):1557–1561, April 2000. doi: 10.1212/wnl.54.8.1557. URL <https://doi.org/10.1212/wnl.54.8.1557>.
- Li, X., Dvornek, N. C., Zhou, Y., Zhuang, J., Ventola, P., and Duncan, J. S. Efficient Interpretation of Deep Learning Models Using Graph Structure and Cooperative Game Theory: Application to ASD Biomarker Discovery. In *Lecture Notes in Computer Science (including subseries Lecture Notes in Artificial Intelligence*

- and *Lecture Notes in Bioinformatics*), volume 11492 LNCS, pp. 718–730. Springer, Cham, jun 2019. ISBN 9783030203504. doi: 10.1007/978-3-030-20351-1_56. URL http://link.springer.com/10.1007/978-3-030-20351-1_{_}56.
- Long, R. K. M., Moriarty, K. P., Cardoen, B., Gao, G., Vogl, A. W., Jean, F., Hamarneh, G., and Nabi, I. R. Super resolution microscopy and deep learning identify zika virus reorganization of the endoplasmic reticulum. *Scientific Reports*, 10(1), December 2020. doi: 10.1038/s41598-020-77170-3. URL <https://doi.org/10.1038/s41598-020-77170-3>.
- Madani, A., Arnaout, R., Mofrad, M., and Arnaout, R. Fast and accurate view classification of echocardiograms using deep learning. *npj Digital Medicine*, 1(1), March 2018. doi: 10.1038/s41746-017-0013-1. URL <https://doi.org/10.1038/s41746-017-0013-1>.
- Martí-Bonmatí, L., Sopena, R., Bartumeus, P., and Sopena, P. Multimodality imaging techniques. *Contrast Media & Molecular Imaging*, 5(4):180–189, July 2010. doi: 10.1002/cmml.393. URL <https://doi.org/10.1002/cmml.393>.
- Menze, B. H., Jakab, A., Bauer, S., Kalpathy-Cramer, J., Farahani, K., Kirby, J., Burren, Y., Porz, N., Slotboom, J., Wiest, R., Lanczi, L., Gerstner, E., Weber, M.-A., Arbel, T., Avants, B. B., Ayache, N., Buendia, P., Collins, D. L., Cordier, N., Corso, J. J., Criminisi, A., Das, T., Delingette, H., Demiralp, ., Durst, C. R., Dojat, M., Doyle, S., Festa, J., Forbes, F., Geremia, E., Glocker, B., Golland, P., Guo, X., Hamamci, A., Iftekharuddin, K. M., Jena, R., John, N. M., Konukoglu, E., Lashkari, D., Mariz, J. A., Meier, R., Pereira, S., Precup, D., Price, S. J., Raviv, T. R., Reza, S. M. S., Ryan, M., Sarikaya, D., Schwartz, L., Shin, H.-C., Shotton, J., Silva, C. A., Sousa, N., Subbanna, N. K., Szekely, G., Taylor, T. J., Thomas, O. M., Tustison, N. J., Unal, G., Vasseur, F., Wintermark, M., Ye, D. H., Zhao, L., Zhao, B., Zikic, D., Prastawa, M., Reyes, M., and Van Leemput, K. The multimodal brain tumor image segmentation benchmark (BRATS). *IEEE Transactions on Medical Imaging*, 34(10):1993–2024, October 2015. doi: 10.1109/tmi.2014.2377694. URL <https://doi.org/10.1109/tmi.2014.2377694>.
- Patel, A., Silverberg, C., Becker-Weidman, D., Roth, C., and Deshmukh, S. Understanding body MRI sequences and their ability to characterize tissues. *Universal Journal of Medical Science*, 4(1):1–9, January 2016. doi: 10.13189/ujmsj.2016.040101. URL <https://doi.org/10.13189/ujmsj.2016.040101>.
- Pereira, S., Meier, R., Alves, V., Reyes, M., and Silva, C. A. Automatic brain tumor grading from mri data using convolutional neural networks and quality assessment. In Stoyanov, D., Taylor, Z., Kia, S. M., Oguz, I., Reyes, M., Martel, A., Maier-Hein, L., Marquand, A. F., Duchesnay, E., Löfstedt, T., Landman, B., Cardoso, M. J., Silva, C. A., Pereira, S., and Meier, R. (eds.), *Understanding and Interpreting Machine Learning in Medical Image Computing Applications*, pp. 106–114, Cham, 2018. Springer International Publishing. ISBN 978-3-030-02628-8.
- Rajpurkar, P., Irvin, J., Ball, R. L., Zhu, K., Yang, B., Mehta, H., Duan, T., Ding, D., Bagul, A., Langlotz, C. P., Patel, B. N., Yeom, K. W., Shpanskaya, K., Blankenberg, F. G., Seekins, J., Amrhein, T. J., Mong, D. A., Halabi, S. S., Zucker, E. J., Ng, A. Y., and Lungren, M. P. Deep learning for chest radiograph diagnosis: A retrospective comparison of the CheXNeXt algorithm to practicing radiologists. *PLOS Medicine*, 15(11):e1002686, November 2018. doi: 10.1371/journal.pmed.1002686. URL <https://doi.org/10.1371/journal.pmed.1002686>.
- Ray, K. Modelling human stomach development with gastric organoids. *Nature Reviews Gastroenterology & Hepatology*, 14(2):68–68, January 2017. doi: 10.1038/nrgastro.2017.4. URL <https://doi.org/10.1038/nrgastro.2017.4>.
- Reyes, M., Meier, R., Pereira, S., Silva, C. A., Dahlweid, F.-M., von Tengg-Kobligk, H., Summers, R. M., and Wiest, R. On the interpretability of artificial intelligence in radiology: Challenges and opportunities. *Radiology: Artificial Intelligence*, 2(3):e190043, May 2020. doi: 10.1148/ryai.2020190043. URL <https://doi.org/10.1148/ryai.2020190043>.
- Ribeiro, M. T., Singh, S., and Guestrin, C. "Why Should I Trust You?": Explaining the Predictions of Any Classifier. In *Proceedings of the 22nd ACM SIGKDD International Conference on Knowledge Discovery and Data Mining - KDD '16*, pp. 1135–1144, New York, New York, USA, 2016. ACM Press. ISBN 9781450342322. doi: 10.1145/2939672.2939778. URL <http://dl.acm.org/citation.cfm?doid=2939672.2939778>.
- Shapley, L. S. *Notes on the n-Person Game – II: The Value of an n-Person Game*. RAND Corporation, Santa Monica, CA, 1951.
- Shen, D., Wu, G., and Suk, H.-I. Deep learning in medical image analysis. *Annual Review of Biomedical Engineering*, 19(1):221–248, June 2017. doi: 10.1146/annurev-bioeng-071516-044442. URL <https://doi.org/10.1146/annurev-bioeng-071516-044442>.
- Singh, A., Sengupta, S., and Lakshminarayanan, V. Explainable deep learning models in medical image analysis. *Journal of Imaging*, 6(6):52, June 2020. doi:

- 10.3390/jimaging6060052. URL <https://doi.org/10.3390/jimaging6060052>.
- Smilkov, D., Thorat, N., Kim, B., Vigas, F., and Wattenberg, M. Smoothgrad: removing noise by adding noise, 2017.
- Song, Y., Treanor, D., Bulpitt, A., and Magee, D. 3d reconstruction of multiple stained histology images. *Journal of Pathology Informatics*, 4(2):7, 2013. doi: 10.4103/2153-3539.109864. URL <https://doi.org/10.4103/2153-3539.109864>.
- Taghanaki, S. A., Havaei, M., Berthier, T., Dutil, F., Di Jorio, L., Hamarneh, G., and Bengio, Y. Infomask: Masked variational latent representation to localize chest disease. In Shen, D., Liu, T., Peters, T. M., Staib, L. H., Essert, C., Zhou, S., Yap, P.-T., and Khan, A. (eds.), *Medical Image Computing and Computer Assisted Intervention – MICCAI 2019*, pp. 739–747, Cham, 2019. Springer International Publishing. ISBN 978-3-030-32226-7.
- Tonekaboni, S., Joshi, S., McCradden, M. D., and Goldenberg, A. What clinicians want: Contextualizing explainable machine learning for clinical end use. In Doshi-Velez, F., Fackler, J., Jung, K., Kale, D., Ranganath, R., Wallace, B., and Wiens, J. (eds.), *Proceedings of the 4th Machine Learning for Healthcare Conference*, volume 106 of *Proceedings of Machine Learning Research*, pp. 359–380, Ann Arbor, Michigan, 09–10 Aug 2019. PMLR. URL <http://proceedings.mlr.press/v106/tonekaboni19a.html>.
- Topol, E. J. High-performance medicine: the convergence of human and artificial intelligence. *Nature Medicine*, 25(1):44–56, 2019. ISSN 1546-170X. doi: 10.1038/s41591-018-0300-7. URL <https://doi.org/10.1038/s41591-018-0300-7>.
- UpToDate. Classification and pathologic diagnosis of gliomas. URL <https://www.uptodate.com/contents/classification-and-pathologic-diagnosis-of-gliomas>.
- Viviano, J. D., Simpson, B., Dutil, F., Bengio, Y., and Cohen, J. P. Saliency is a possible red herring when diagnosing poor generalization. In *International Conference on Learning Representations*, 2021. URL <https://openreview.net/forum?id=c9-WeM-ceB>.
- Wang, D., Wang, L., Zhang, Z., Wang, D., Zhu, H., Gao, Y., Fan, X., and Tian, F. "brilliant ai doctor" in rural china: Tensions and challenges in ai-powered cdss deployment. 2021. doi: 10.1145/3411764.3445432.
- Wang, X., Peng, Y., Lu, L., Lu, Z., Bagheri, M., and Summers, R. M. ChestX-ray8: Hospital-scale chest X-ray database and benchmarks on weakly-supervised classification and localization of common thorax diseases. *Proceedings - 30th IEEE Conference on Computer Vision and Pattern Recognition, CVPR 2017*, 2017-Janua:3462–3471, 2017. doi: 10.1109/CVPR.2017.369.
- Woo, C.-W., Chang, L. J., Lindquist, M. A., and Wager, T. D. Building better biomarkers: brain models in translational neuroimaging. *Nature Neuroscience*, 20(3):365–377, February 2017. doi: 10.1038/nn.4478. URL <https://doi.org/10.1038/nn.4478>.
- Xie, Y., Chen, M., Kao, D., Gao, G., and Chen, X. ' . CheXplain. In *Proceedings of the 2020 CHI Conference on Human Factors in Computing Systems*. ACM, April 2020. doi: 10.1145/3313831.3376807. URL <https://doi.org/10.1145/3313831.3376807>.
- Xu, Y. Deep learning in multimodal medical image analysis. In Wang, H., Siuly, S., Zhou, R., Martin-Sanchez, F., Zhang, Y., and Huang, Z. (eds.), *Health Information Science*, pp. 193–200, Cham, 2019. Springer International Publishing. ISBN 978-3-030-32962-4.
- Yeh, C.-K., Hsieh, C.-Y., Suggala, A., Inouye, D. I., and Ravikumar, P. K. On the (in)fidelity and sensitivity of explanations. In Wallach, H., Larochelle, H., Beygelzimer, A., d'Alché-Buc, F., Fox, E., and Garnett, R. (eds.), *Advances in Neural Information Processing Systems*, volume 32. Curran Associates, Inc., 2019. URL <https://proceedings.neurips.cc/paper/2019/file/a7471fdc77b3435276507cc8f2dc2569-Paper.pdf>.
- Zech, J. R., Badgeley, M. A., Liu, M., Costa, A. B., Titano, J. J., and Oermann, E. K. Variable generalization performance of a deep learning model to detect pneumonia in chest radiographs: A cross-sectional study. *PLOS Medicine*, 15(11):e1002683, November 2018. doi: 10.1371/journal.pmed.1002683. URL <https://doi.org/10.1371/journal.pmed.1002683>.
- Zhang, Y., Vera Liao, Q., and Bellamy, R. K. Effect of confidence and explanation on accuracy and trust calibration in AI-assisted decision making. *FAT* 2020 - Proceedings of the 2020 Conference on Fairness, Accountability, and Transparency*, pp. 295–305, 2020. doi: 10.1145/3351095.3372852.
- Zherebtsov, E., Dremin, V., Popov, A., Doronin, A., Kurakina, D., Kirillin, M., Meglinski, I., and Bykov, A. Hyperspectral imaging of human skin aided by artificial neural networks. *Biomedical Optics Express*, 10(7): 3545, June 2019. doi: 10.1364/boe.10.003545. URL <https://doi.org/10.1364/boe.10.003545>.

Zhou, B., Khosla, A., Lapedriza, A., Oliva, A., and Torralba, A. Learning deep features for discriminative localization. In *2016 IEEE Conference on Computer Vision and Pattern Recognition (CVPR)*, pp. 2921–2929, 2016. doi: 10.1109/CVPR.2016.319.